

## Bismuth labeling for the CT assessment of local administration of magnetic nanoparticles

This content has been downloaded from IOPscience. Please scroll down to see the full text.

2015 Nanotechnology 26 135101

(<http://iopscience.iop.org/0957-4484/26/13/135101>)

View [the table of contents for this issue](#), or go to the [journal homepage](#) for more

Download details:

IP Address: 150.244.102.69

This content was downloaded on 12/03/2015 at 09:05

Please note that [terms and conditions apply](#).

# Bismuth labeling for the CT assessment of local administration of magnetic nanoparticles

S Veintemillas-Verdaguer<sup>1</sup>, Y Luengo<sup>1</sup>, C J Serna<sup>1</sup>, M Andrés-Vergés<sup>2</sup>,  
M Varela<sup>3,4</sup>, Macarena Calero<sup>5,6</sup>, Ana Lazaro-Carrillo<sup>5,6</sup>,  
Angeles Villanueva<sup>5,6</sup>, A Sisniega<sup>7</sup>, P Montesinos<sup>8</sup> and M P Morales<sup>1</sup>

<sup>1</sup> Instituto de Ciencia de Materiales de Madrid, CSIC, Sor Juana Inés de la Cruz 3, Cantoblanco, 28049, Madrid, Spain

<sup>2</sup> Departamento de Química Orgánica e Inorgánica, Facultad de Ciencias UEX, Avda de Elvás s/n, 06006, Badajoz, Spain

<sup>3</sup> Materials Science & Technology Division, Oak Ridge National Laboratory, Oak Ridge, TN 37831 USA

<sup>4</sup> Departamento de Física Aplicada III & Instituto Pluridisciplinar, Universidad Complutense de Madrid, 28040, Madrid, Spain

<sup>5</sup> Departamento de Biología, Universidad Autónoma de Madrid, Darwin 2, Cantoblanco, 28049, Madrid, Spain

<sup>6</sup> IMDEA Nanociencia, Faraday 9, Cantoblanco, Madrid, Spain

<sup>7</sup> Departamento de Bioingeniería e Ingeniería Aeroespacial, Universidad Carlos III de Madrid, Spain

<sup>8</sup> Instituto de Investigación Sanitaria Gregorio Marañón (IiSGM), Madrid, Spain

E-mail: [sabino@icmm.csic.es](mailto:sabino@icmm.csic.es) (S Veintemillas-Verdaguer)

Received 12 December 2014, revised 10 February 2015

Accepted for publication 14 February 2015


Published 11 March 2015



CrossMark

## Abstract

Many therapeutic applications of magnetic nanoparticles involve the local administration of nanometric iron oxide based materials as seeds for magnetothermia or drug carriers. A simple and widespread way of controlling the process using x-ray computed tomography (CT) scanners is desirable. The combination of iron and bismuth in one entity will increase the attenuation of x-rays, offering such a possibility. In order to check this possibility core-shell nanocrystals of iron oxide@bismuth oxide have been synthesized by an aqueous route and stabilized in water by polyethylene glycol (PEG), and we have evaluated their ability to generate contrast by CT and magnetic resonance imaging (MRI) to measure the radiopacity and proton relaxivities using phantoms. High-resolution scanning transmission electron microscopy (STEM) revealed that the material consists of a highly crystalline 8 nm core of maghemite and a 1 nm shell of bismuth atoms either isolated or clustered on the nanocrystal's surface. The comparison of  $\mu$ CT and MRI images of mice acquired in the presence of the contrast shows that when local accumulations of the magnetic nanoparticles take place, CT images are more superior in the localization of the magnetic nanoparticles than MRI images, which results in magnetic field inhomogeneity artifacts.

 Online supplementary data available from [stacks.iop.org/NANO/26/135101/mmedia](http://stacks.iop.org/NANO/26/135101/mmedia)

Keywords: iron bismuth nanocrystals, surface modification, magnetic properties, radiopacity, computed tomography, magnetic resonance imaging

(Some figures may appear in colour only in the online journal)

## 1. Introduction

Computed tomography (CT) is a widely available tool for medical imaging that due to the small differences in attenuation of x-ray of soft tissues need contrast agents. The design of colloidal systems able to actuate as contrast agents for this technique is desirable since when properly functionalized, they could have much longer circulation times in blood than iodine-based molecular agents and present a less harmful elimination route [1]. In addition, the evolution of nanoparticle synthesis methods now allow them to vary not only their composition but also their size, shape and surface chemistry, with the possibility of integrating several functionalities in one entity [2]. Several nanoparticulated CT contrast agents have been reported based on iodine functionalized polymers [3], gold nanoparticles [4], core-shell iron oxide/tantalum oxide nanoparticles [5] and iron-platinum alloy nanoparticles [6]. Nanoparticulated CT contrasts bearing bismuth, in particular bismuth sulphide nanodots (2–3 nm) [8–11], have obtained special attention due to a combination of low price, low toxicity and a high x-ray attenuation coefficient [2, 7]. This material has been successfully prepared in large quantities and targeted to contrast breast cancer [10]. Nanoplatelets of bismuth selenide were also employed as a theranostic platform for CT imaging and photodynamic treatment of cancer in an animal model [12], and bismuth oxide/oxychloride-loaded 50 nm long nanotubes were employed for stem cell imaging [13]. Metallic iron-bismuth magnetic nanoparticles were recently synthesized by the soft chemistry route, and their complex growth mechanism was revealed [14].

Recently, we successfully prepared core-shell iron oxide/bismuth oxide nanocrystals by an aqueous solution method which allows tuning magnetic nanoparticle size and bismuth content up to 17%, keeping the uniformity in size and shape of the nanoparticles and keeping a high crystallinity [15]. The aim of this work is to use this material as a model for the use of bismuth as a label for magnetic nanomaterials and to explore the possibilities of this material for being imaged by MRI and CT medical scanners. To this purpose we have doubly coated the nanocrystals with silica and a silica-PEG polymer to obtain stable colloidal suspensions at a physiological pH and to slow down the possible release of bismuth. The dispersion has been characterized from the physico-chemical point of view, the cell toxicity has been evaluated, the relaxivities and x-ray attenuation have been measured *in vitro* and a comparative CT and MR image study using an animal model has been carried out.

## 2. Materials and methods

### 2.1. Materials

The silane polyethylene glycol derivative (m-PEG silane®) MW 5000 was purchased from Lysan Bio., Inc. The iodine-based contrast Xenetix® was supplied courtesy of Guerbet

Group; the rest of the reagents were of analytical grade purchased from Sigma-Aldrich and were used as received.

### 2.2. Characterization

Nanoparticle size and size distribution were characterized by transmission electron microscopy (TEM) using a JEOL-2000 FXII apparatus operated at 200 KeV. A drop of the suspensions was deposited onto a carbon-coated copper grid and left to evaporate at room temperature. The mean size ( $D$ ) and the standard deviation ( $SD$ ) were evaluated from the electron micrographs by counting around 500 particles. A close view of the nanocrystals was done by high-resolution STEM using a Nion UltraSTEM200 dedicated STEM operated at 200 keV and the high angle annular dark field (HAADF) imaging technique, which is sensitive to the square power of the atomic number (approximately). As a result iron and bismuth atoms could be easily distinguished.

The dried aqueous dispersions were characterized by infrared spectroscopy in KBr pellets (Bruker IFS 66V-S), by x-ray diffraction (Powder Diffractometer Bruker D8 Advance with Cu  $K\alpha$  radiation with energy-discriminator SOLX) and by thermogravimetry under 100 sccm of air flow and  $0.5\text{ }^{\circ}\text{C min}^{-1}$  (Thermal Analysis ATD/DSC/TG model Q600 TA Instruments®).

The magnetic properties of the dried samples were determined using a vibrating sample magnetometer (VSM) (MLVSM9 MagLab 9T, Oxford Instruments) with a saturating field of 5 T. The magnetization values were normalized to the amount of hybrid material (FeBi) to obtain the specific magnetization (emu/g). Saturation magnetization ( $M_s$ ) was determined by  $H^{-1}$  extrapolation of the magnetization values in the high field region where a linear increase in the magnetization is observed.

The composition of the aqueous dispersions in iron and bismuth was measured after the dissolution of the sample in diluted hydrofluoric acid by inductively coupled plasma mass spectrometry (ICP-MS). The hydrodynamic size of the dispersions and zeta potential was determined by photon correlation spectroscopy (PCS) using a Zetasizer Nano ZS® (Malvern Instruments Ltd).

### 2.3. Synthesis and coating of core/shell magnetite/bismuth oxide nanocrystals

Core-shell bismuth-oxide-capped iron oxide nanocrystals were prepared by oxidative precipitation [15]. The particular product used in this study was prepared as follows: 180 mL of ethanol/water at 50% vol containing NaOH and  $\text{NaNO}_3$  and 20 mL of  $\text{H}_2\text{SO}_4$  0.2 M containing carefully deoxygenated  $\text{FeSO}_4$  and  $\text{Bi}(\text{NO}_3)_3$  were mixed in a three-neck round bottom flask placed in an oil bath with mechanical stirring and with flowing nitrogen. The concentrations of the reactants after mixing were  $6.6 \times 10^{-2}$  M NaOH, 0.05 M  $\text{NaNO}_3$ ,  $2.5 \times 10^{-3}$  M  $\text{FeSO}_4$  and  $5 \times 10^{-4}$  M  $\text{Bi}(\text{NO}_3)_3$ . That gives a Bi/Fe atom ratio of 0.20 determined by ICP-MS; this proportion is close to the maximum attainable without segregation of iron and bismuth oxides [15]. The system was

maintained at 90 °C for 24 h unstirred. After that, the solution was left to cool at room temperature, and the solid (FeBi) was separated by magnetic decantation and washed several times with distilled water.

In order to obtain a stable dispersion of these core-shell nanocrystals, we first encapsulated the materials in silica after we coated them with polyethylene glycol using m-PEG silane®. The complete procedure is as follows: 15 mL of FeBi (274 mg) were added drop-wise to a solution of 900 mL 2-propanol + 22 mL NH<sub>4</sub>OH (30% NH<sub>3</sub>) + 440 µL tetraethoxy silane (TEOS) under bubbling nitrogen and mechanical stirring. The dispersion was stirred for 1 h to promote the hydrolysis of TEOS. The silica-coated FeBi aggregates were washed three times with 2-propanol using magnetic separation or mild centrifugation (2000 rcf and 2 h). The solvent was then changed to acetonitrile and washed three times using centrifugation. The final volume of the dispersion was 100 mL. For the grafting process the previously mentioned dispersion was treated with 1.5 g of m-PEG silane® dissolved in 150 mL acetonitrile and 35 mL water. The dispersion was mechanically stirred (orbital stirrer) for 3 h. After the grafting process the suspension (FeBi@SiPEG) was washed three times with acetonitrile, one time with a mixture of acetonitrile/water at 50% vol and three times with water. The final volume of the dispersion was 40 mL. In order to refine the dispersions, the aggregates were separated by centrifugation at 11 rcf for 10 min. Finally, the dispersion was repeatedly dialyzed for 24 h each time in 5 L of distilled water using a 10 000 nominal cut-off molecular weight membrane. In order to make the suspension suitable for subcutaneous administration it was made with 1 mM in tri-sodium citrate and made sterile by filtration through 0.22 µm or by γ-ray irradiation with 25 KGy using standard procedures.

#### 2.4. Measurement of the <sup>1</sup>H water relaxation times T<sub>1</sub> and T<sub>2</sub> and x-ray attenuation

In order to evaluate the efficiency of the suspensions as contrast agents for MRI measurements of the relaxation times of water protons in the presence of FeBi@SiPEG were carried out in a time-domain NMR benchtop system MINISPEC MQ60 (Bruker) at 37 °C and 1.5 T using standard methods. The relaxivities  $r_1$  and  $r_2$  (s<sup>-1</sup> mMFe<sup>-1</sup>) were obtained from the measured longitudinal and transversal relaxation times  $T_1$  and  $T_2$  of gelified (agar 0.5%) dispersions of FeBi@SiPEG at concentrations below 1 mM Fe from the linear plot of  $1/T_1$  and  $1/T_2$  as a function of the concentration.

The x-ray attenuation coefficient of the aqueous dispersions of FeBi@SiPEG nanocrystals was obtained from the images of water dispersions of the nanocrystals at different concentrations obtained with two x-ray µ-CT systems, one working at 50 kV (Argus® PET/CT, Sedecal S.A.) and the other working at 110 kV in an in-house developed system. To cover the most important x-ray contrast usage scenarios, two different x-ray beam spectra were used: one usually employed in small-animal preclinical imaging (peak energy of 50 kVp and 1 mm Al added filtration) and the second one closer to those employed in the clinical practice (110 kVp peak energy

and 0.2 mm Cu added filtration). The images were reconstructed using the Feldkamp–Davis–Kess (FDK) algorithm [16]. The attenuation values were estimated from 20×20 pixel regions of interest (ROIs) placed on a coronal slice of the reconstructed volume over homogeneous areas of the contrast media. To be used as a reference for the measured values, several dilutions of iodine-based contrast Xenetix® and pure iron oxide nanocrystals were also measured for the same approximate range of concentrations.

#### 2.5. Cellular uptake

*In vitro* studies were carried out in a human cervix adenocarcinoma (HeLa) cell line. The cells were grown as monolayer cultures in Dulbecco's modified Eagle's medium (DMEM), supplemented with 10% (v/v) foetal bovine serum (FBS), 50 units/mL penicillin and 50 µg mL<sup>-1</sup> streptomycin in a humidified atmosphere containing 5% CO<sub>2</sub> at 37 °C. The cells were seeded in 24-well plates with or without 10 mm square coverslips. The subconfluent HeLa cells were incubated with different concentrations of FeBi@SiPEG (0.05 mgFe mL<sup>-1</sup>, 0.01 mgBi mL<sup>-1</sup>; 0.1 mgFe mL<sup>-1</sup>, 0.02 mgBi mL<sup>-1</sup>; and 0.5 mgFe mL<sup>-1</sup>, 0.1 mgBi mL<sup>-1</sup>, all in a culture medium) for 24 and 48 h.

The nanoparticle uptake and intracellular distribution were qualitatively monitored via Prussian blue staining for iron detection. Briefly, the cells preincubated with different concentrations of nanoparticles for 24 or 48 h and were fixed in methanol at -20 °C for 5 min, stained with an equal volume of 4% HCl and 4% KMnO<sub>4</sub> for 15 min and counterstained with 0.5% neutral red for 2 min. The preparations were then washed with distilled water, air dried and mounted in a DePeX® medium.

The colorimetric ferrozine assay was performed for intracellular iron quantitation [17]. The HeLa cells seeded in 24-well plates were incubated with different concentrations of nanoparticles (0.05 mgFe mL<sup>-1</sup>, 0.01 mgBi mL<sup>-1</sup>; 0.1 mgFe mL<sup>-1</sup>, 0.02 mgBi mL<sup>-1</sup>; and 0.5 mgFe mL<sup>-1</sup>, 0.1 mgBi mL<sup>-1</sup>, all in a culture medium) for 24 h, followed by three washes with phosphate-buffered saline (PBS). After completely removing the PBS, cells in three wells were trypsinized and counted to determine the number of cells per well. The cells in the other three wells were frozen at -20 °C for 1 h and then 500 µL of 50 nM NaOH were added to each well for 2 h in a hummed movement camera. Aliquots of cell lysates were transferred to 1.5 mL eppendorf and mixed with 500 µL of 10 mM HCl and 500 µL of iron-releasing reagent consisting of a freshly mixed solution of equal volumes of 1.4 M HCl and 4.5% (w/v) KMnO<sub>4</sub> in H<sub>2</sub>O. Then, the mixtures were incubated for 2 h at 60 °C within a fume hood since chlorine gas is produced during the reaction. The samples were left to cool to room temperature, and 150 µL of an iron-detection reagent (6.5 mM ferrozine, 6.5 mM neocuproine, 2.5 M ammonium acetate and 1 M ascorbic acid, all dissolved in water) were added to each tube. After 30 min, 500 µL of the solution obtained in each tube was transferred into a well of a 24-well plate, and the absorbance was measured at 570 nm in a SpectraFluor® spectrophotometer

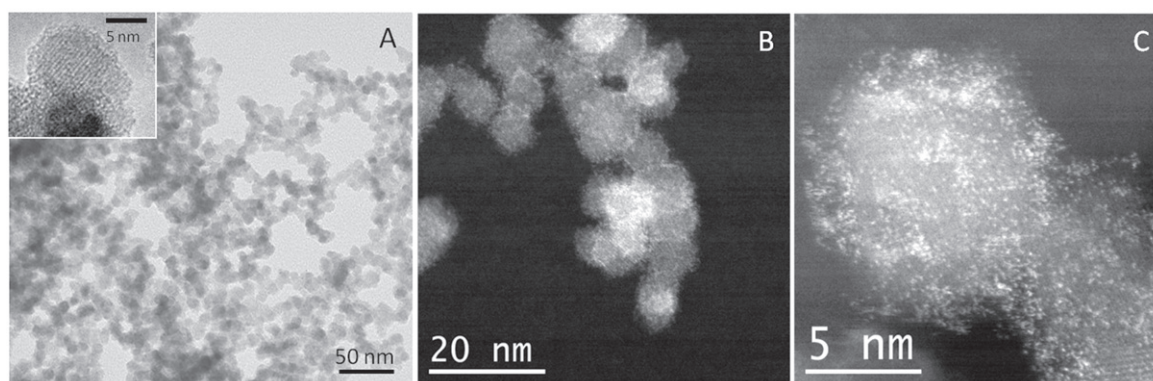


**Figure 1.** Bright-field and HAADF images of FeBi nanocrystals (the bright points on figures 1(B) and (C) correspond to bismuth atoms).

(TECAN Group Ltd). The iron content of the sample was calculated by comparing its absorbance to that of a range of standard concentrations of equal volume that had been prepared in a way similar to that of the sample (mixture of 100  $\mu\text{L}$  of  $\text{FeCl}_3$  standards (0–300  $\mu\text{M}$ ), 100  $\mu\text{L}$  of a solution 10 mM HCl, 50 mM NaOH, 500  $\mu\text{L}$  of the releasing reagent and 1500  $\mu\text{L}$  detection reagent). The intracellular iron concentration determined for each well of a cell culture was normalized against the number of cells per well.

## 2.6. Cytotoxicity

Cell survival was evaluated by a standard methyl thiazolium bromide (MTT) assay and a trypan blue exclusion test. For the MTT assay, HeLa cells seeded in 24-well plates were incubated with nanoparticles at different concentrations (0.05 mgFe mL<sup>-1</sup>, 0.01 mgBi mL<sup>-1</sup>; 0.1 mgFe mL<sup>-1</sup>, 0.02 mgBi mL<sup>-1</sup>; and 0.5 mgFe mL<sup>-1</sup>, 0.1 mgBi mL<sup>-1</sup>) for 24 h. Then, the cells were washed three times with PBS and incubated for another 24 h in a culture medium (without nanoparticles). The viability of the HeLa cells was determined using a MTT assay [18]. Briefly, dimethylthiazolyl-diphenyl-tetrazolium bromide was added to each well to a final concentration of 50  $\mu\text{g mL}^{-1}$ . The cells were incubated for 3 h, and the formazan obtained was dissolved, adding 0.5 mL of dimethylsulfoxide (DMSO) in each well. Finally, the optical density was measured at 542 nm. Cell survival was expressed as a percentage of the absorption of treated cells in comparison with that of control cells (not incubated with nanoparticles). The results obtained are the mean value and standard deviation (SD) from at least six experiments. A statistical analysis was performed by GraphPad Prism Software (CA, USA) using one-way analysis of variance (ANOVA) and Tukey's test. The threshold for significance was  $P=0.05$ , and the  $P$  values  $<0.05$ ,  $<0.01$  and  $<0.005$  were considered as significant and named with (\*), (\*\*) and (\*\*\*) respectively.

The cell viability was also quantified by the trypan blue dye exclusion method. Briefly, after 24 h of incubation with FeBi@SiPEG, trypsin was added to the control and treated cells. After the cells were detached from the plate, they were resuspended in a culture media. Equal volumes of each cell suspension and the trypan blue solution (0.2% in PBS) were

mixed and used for cell counting by means of a hemocytometer. The blue-stained cells were considered as nonviable, and the unstained cells were considered as viable.

## 2.7. Image study

The animal (an *ex vivo* 30 g weight mouse) received a subcutaneous injection of 100  $\mu\text{L}$  of FeBi@SiPEG dispersion in the left hind leg (29 mgFe Kg<sup>-1</sup> B.W., 10 mgBi Kg<sup>-1</sup> B.W.). The study was performed with a small-animal scanner for positron electron tomography and CT (PET/CT) (Argus® PET/CT, Sedecal S.A.) and with a preclinical 7 T MRI system (Biospin®, Bruker). The CT study was acquired using an x-ray beam current of 240  $\mu\text{A}$  and a tube voltage of 40 kV under similar conditions as the attenuation study. An axial MRI was acquired using a segmented gradient echo (SNAP) sequence operating in fast imaging with steady state precession (FISP) mode using a linear volume coil and with the following parameters: echo time (TE) 2 ms, repetition time (TR) 300 ms, field of view (FOV) 4  $\times$  2.5 cm<sup>2</sup>, matrix size 192  $\times$  192 mm<sup>2</sup>, slice thickness of 0.9 mm and an acquisition time of 5 min.

## 3. Results

### 3.1. Characterization of the iron bismuth nanoparticles

The chemical analysis of the sample presents a Bi/Fe atomic ratio of 0.19 that matches the atomic ratio of the reaction mixture. The standard observation of the FeBi nanocrystals by TEM (figure 1(A)) shows that the sample is homogeneous in size and shape with  $8 \pm 1$  nm size (Supplementary Information). The inset in figure 1(A) shows the core-shell structure of the nanocrystals in which the core, identified as pure iron oxide [15, 19], presents a high crystalline quality in contrast to the bismuth-bearing shell that appears to be more disordered. In order to gain more information on the microstructure of this material, we performed an electron microscopy study employing the HAADF technique (figures 1(B) and (C)). In these figures the heavier Bi atoms (not distinguishable under ordinary TEM observation) appear brighter than the Fe atoms. The bismuth-bearing shell now appears discontinuous with the Bi atoms distributed as isolated

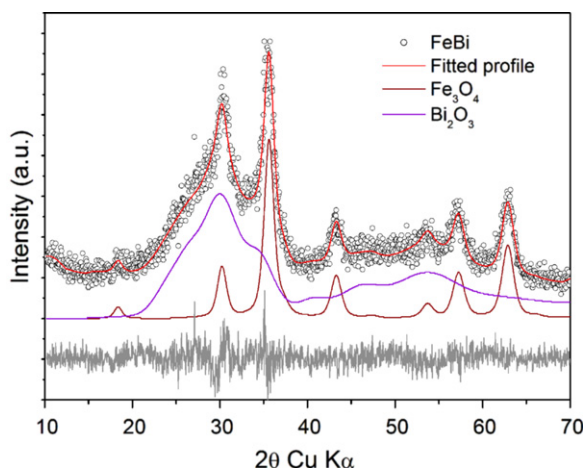


**Figure 2.** X-ray powder diffraction of FeBi core-shell nanocrystals showing the  $\text{Fe}_3\text{O}_4$  and  $\text{Bi}_2\text{O}_3$  components.

surface atoms or in small clusters of presumably bismuth oxide. Recently, a similar sample than was employed in this work, studied by x-ray absorption spectroscopy (XAS), revealed that the Bi atoms do not form a well-defined Bi oxide structure and that the bismuth shell consists in clusters  $[\text{BiO}_{6-x}(\text{OH})_x]$  bonded by hydroxyl bridges to the magnetic core [19]. Nevertheless, in order to fit the x-ray powder diffraction profile of FeBi by means of the Fullprof computer program [20] we used (bismite)  $\alpha\text{-Bi}_2\text{O}_3$  JCPDS N° 76-1730 [21] as the most approximate state of bismuth in the sample and the maghemite ( $\gamma\text{-Fe}_2\text{O}_3$ ) JCPDS N° 39-1346 [22] for the magnetic core. Figure 2 presents the result of the fitting procedure with the superposition of the diffraction patterns corresponding to both phases. The Scherrer sizes calculated using the widths at half height of the deconvoluted peaks were 6.3 nm for maghemite (311) and 2.4 nm for bismite (120). These data are in good agreement with the TEM size, with a nanostructure of iron oxide cores of around 7 nm and with isolated clusters of bismuth atoms of around 1 nm on the surface observed by HRTEM.

The x-ray attenuation was measured on phantoms of different concentrations of FeBi in water and compared with standard iodine-based contrast and pure iron oxide nanoparticles of the same size (figure 3(A)). As expected, the FeBi sample presents the highest opacity against the x-rays measured by the slope of the linear plot of the CT numbers (HU) against the concentration. The differences in attenuation between bismuth and iodine (Xenetix®) were less important at high energies.

### 3.2. Characterization of the coated iron bismuth nanoparticles

A silica coating and further modification with PEG resulted in a stable suspension of SiPEG-coated FeBi aggregates. The aqueous dispersion employed in this study (FeBi@SiPEG) presented a hydrodynamic diameter of  $134 \pm 25$  nm (intensity), a Z potential of  $-29 \pm 6$  mV (pH = 7) and analytical concentrations of iron and bismuth of 157 mM and 14.6 mM, respectively, that gives a Bi/Fe atom ratio of 0.09 ( $8.7 \text{ mgFe mL}^{-1}$ ,  $3.1 \text{ mgBi mL}^{-1}$ ). An important proportion of

bismuth was lost during the coating process due to the weak bonding among the iron oxide and the amorphous bismuth oxohydroxide [19]. The infrared spectrum of dry FeBi@SiPEG (figure 4) shows the stretching Si-O band of silica ( $1008 \text{ cm}^{-1}$ ), the stretching C-H band ( $2919 \text{ cm}^{-1}$ ) and the collective vibrations of the group O-CH<sub>2</sub>-CH<sub>2</sub>-O ( $1400\text{--}1200 \text{ cm}^{-1}$ ,  $950\text{--}850 \text{ cm}^{-1}$ ) that form the helicoidal chain of the polyethyleneglycol [23], confirming the success of the coating process. The thermogravimetric study shows that the amount of polymer grafted onto the surface was 3.7% (supplementary information).

Figure 5 depicts the hysteresis cycles of the coated sample at room temperature and at 5 K. At room temperature the sample presents superparamagnetic behavior with a saturation magnetization of  $48 \text{ emu g}^{-1}$  and, at 5 K, a ferromagnetic behavior with a saturation magnetization of  $57.3 \text{ emu g}^{-1}$  and coercive field of 0.029 T. When those values were corrected for the amount of bismuth, saturation magnetization went up to  $70 \text{ emu g}^{-1}$  and  $75 \text{ emu g}^{-1}$  of iron oxide at 300 K and 5 K, respectively, which are close to the saturation magnetization of bulk maghemite  $76 \text{ emu g}^{-1}$  at 300 K [24].

The relaxometric properties of the aqueous dispersions of FeBi@SiPEG showed values of  $r_1 = 3.65 \text{ s}^{-1} \text{ mMFe}^{-1}$  and  $r_2 = 175 \text{ s}^{-1} \text{ mMFe}^{-1}$  (figure 3(B)), which is similar to most of the commercial superparamagnetic iron oxide (SPIO) nanoparticles employed as contrast agents for MRI [25].

### 3.3. Biological characterization

The intracellular uptake of iron oxide nanoparticles was observed by Prussian blue staining (figure 6(A)). Clearly, the internal amount of iron-containing cytoplasmic blue spots depends on nanoparticle concentration and incubation time. The cells incubated with  $0.05 \text{ mgFe mL}^{-1}$ ,  $0.01 \text{ mgBi mL}^{-1}$  for 24 or 48 h showed insignificant accumulation of nanoparticles (figures 6(A)(b)). In contrast, efficient internalization (100% cell labeling efficiency) was observed after incubation with  $0.1 \text{ mgFe mL}^{-1}$ ,  $0.02 \text{ mgBi mL}^{-1}$ , even though intracellular accumulation after 24 h of incubation was less than for 48 h (figures 6(A)(c), (f)). It is important to note that with these concentrations, nanoparticle aggregation does not occur, and extracellular nanoparticles were not observed. In contrast, aggregated nanoparticles to the cell's surface were detected at a higher concentration ( $0.5 \text{ mgFe mL}^{-1}$ ,  $0.1 \text{ mgBi mL}^{-1}$ ) with the enhanced intracellular internalization of nanoparticles (figures 6(A)(d), (g)). More importantly, cells incubated with FeBi@SiPEG and stained by Prussian blue reaction did not show a significant change in cell morphology related to untreated (control) cells, even after 48 h of incubation. Non-apoptotic morphological abnormalities (such as cell shrinkage, membrane blebbing and nuclear chromatin condensation) or necrotic alterations were observed. These findings suggest that the FeBi@SiPEGs internalized were nontoxic to HeLa cells at the concentration ranges and incubation times used herein.

On the other hand, colorimetric ferrozine-based results corroborated the previous observations (see figure 6(B)). The quantitation of iron into HeLa cells incubated 24 h with

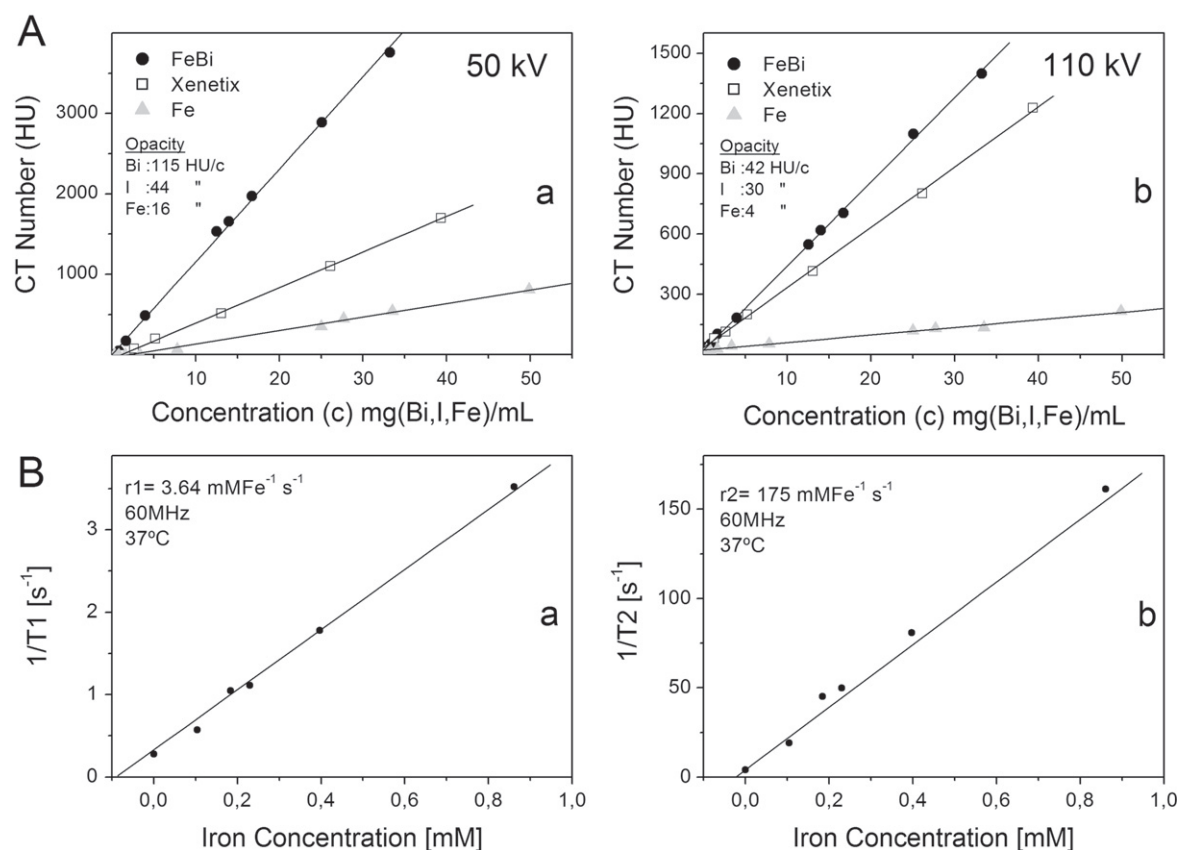


**Figure 3.** Contrast agent characterization. (A) x-ray attenuation of sample FeBi as a function of the bismuth concentration at 50 kV (a) and 110 kV (b) in CT numbers (*HU*),  $HU = 1,000 (\mu - \mu_w) / \mu_w$ , where  $\mu$  and  $\mu_w$  are the linear absorption coefficients of the sample and water, respectively. The iodine-based commercial sample Xenetix 350® (Guerbet, France) and a dispersion of iron oxide (Fe) of the same particle size as FeBi were shown for comparison. (B) Relaxometric plots of the coated sample FeBi@SiPEG for the determination of relaxivities 1/T1 plot (a) and 1/T2 plot (b).

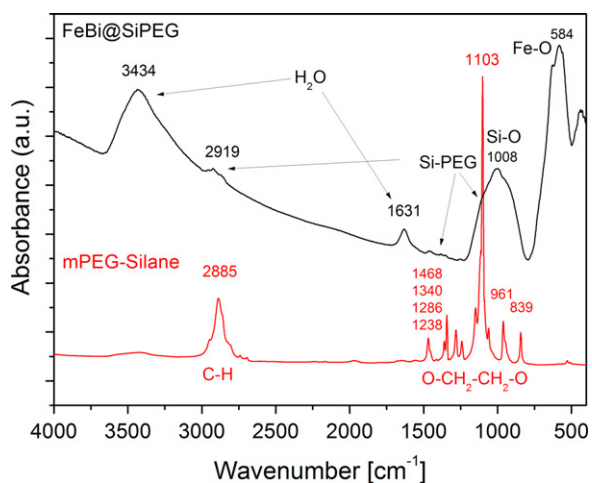


**Figure 4.** Infrared spectrum of the coated sample FeBi@SiPEG; in red: the infrared spectrum of the coating m-PEG Silane<sup>(R)</sup>.

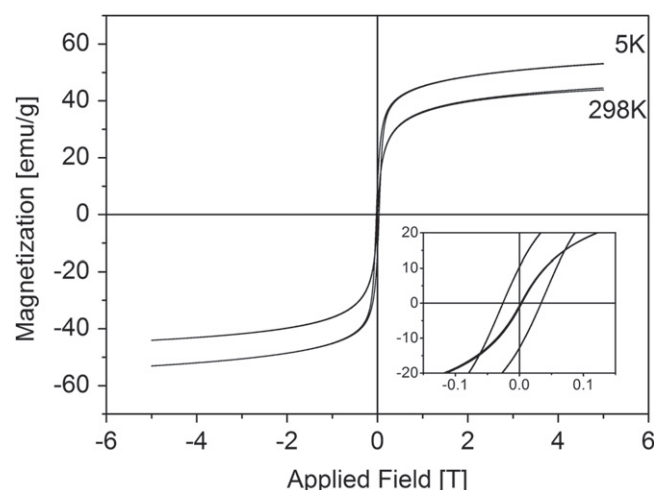


**Figure 5.** Hysteresis cycles of the dry-coated sample FeBi@SiPEG at room temperature and at 5 K.

FeBi@SiPEG at 0.05 mgFe mL<sup>-1</sup>, 0.01 mgBi mL<sup>-1</sup>; 0.1 mgFe mL<sup>-1</sup>, 0.02 mgBi mL<sup>-1</sup>; and 0.5 mgFe mL<sup>-1</sup>, 0.1 mgBi mL<sup>-1</sup> were 4.4 ± 0.9, 9.3 ± 1.2 and 43 ± 1 pg cell<sup>-1</sup>, respectively. The basal amount of iron in untreated HeLa cells were ~3 pg cell<sup>-1</sup>. The statistical evaluation (one-way ANOVA Tukey's test) showed that after 24 h incubation the

nanoparticles' uptake into HeLa cells depends significantly on the concentration. However, the data on the uptake of nanoparticles by cells with 0.5 mgFe mL<sup>-1</sup>, 0.1 mgBi mL<sup>-1</sup> should be somewhat overestimated due to the above-mentioned presence of nanoparticles attached to the cell membrane and not internalized by cells.

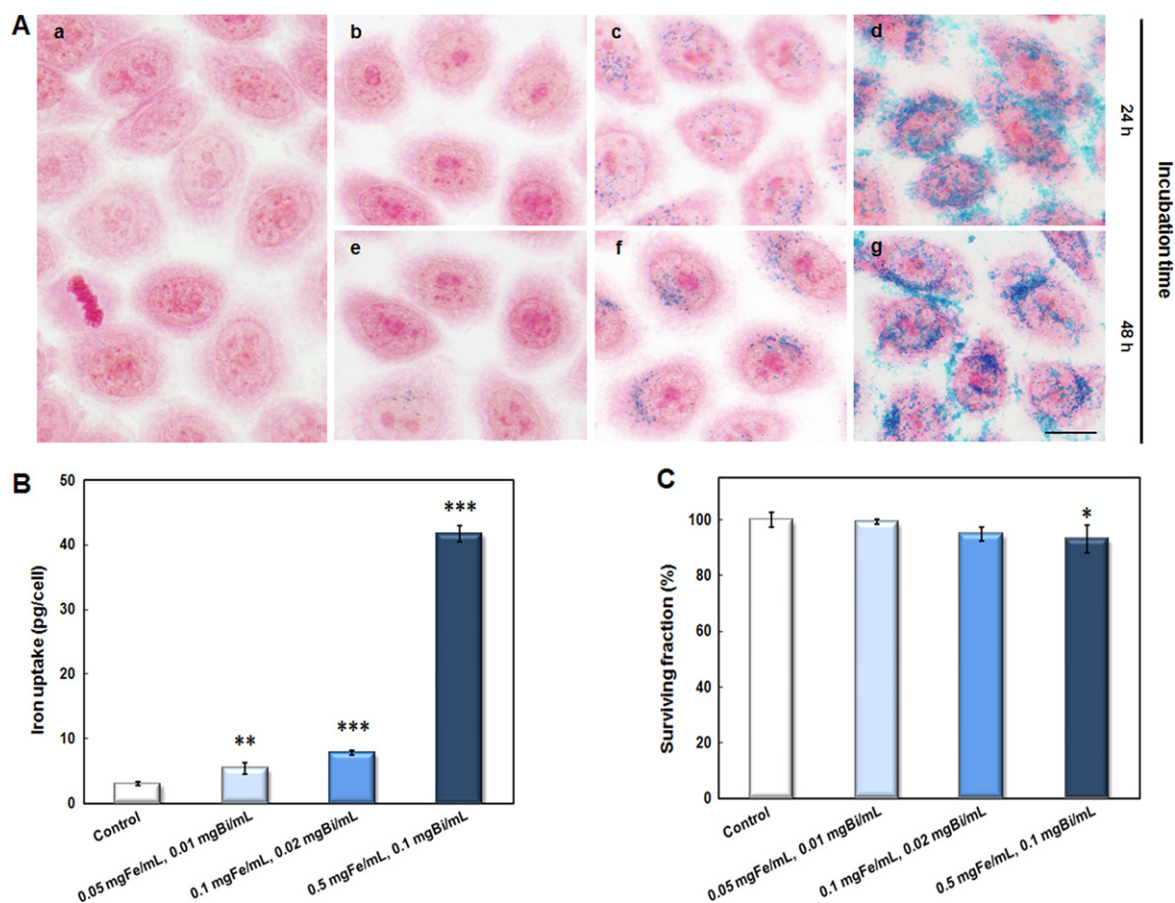


**Figure 6.** Nanoparticle-cell interactions. (A) Images of Prussian blue staining HeLa cells incubated with FeBi@SiPEG at different concentrations and incubation times. (a) Untreated (control) cells; (b)–(d) Cells incubated for 24 h with 0.05 mgFe mL<sup>-1</sup>, 0.01 mgBi mL<sup>-1</sup>, 0.1 mgFe mL<sup>-1</sup>, 0.02 mgBi mL<sup>-1</sup> or 0.5 mgFe mL<sup>-1</sup>, 0.1 mgBi mL<sup>-1</sup>, respectively; (e)–(g) Cells incubated for 48 h with 0.05 mgFe mL<sup>-1</sup>, 0.01 mgBi mL<sup>-1</sup>, 0.1 mgFe mL<sup>-1</sup>, 0.02 mgBi mL<sup>-1</sup> or 0.5 mgFe mL<sup>-1</sup>, 0.1 mgBi mL<sup>-1</sup>, respectively. Scale bar = 10  $\mu$ m. (B) Uptake of nanoparticles by a ferrozine assay. (C) Cytotoxicity of nanoparticles by a MTT test. Representative data from four independent experiments are shown (B) and (C). Data are shown as the mean  $\pm$  SD. In (B) and (C) statistical significance vs control is indicated as \* $P$  < 0.05, \*\* $P$  < 0.01 and \*\*\* $P$  < 0.005.

Finally, MTT assays were performed at 24 h after an incubation time period (24 or 48 h) in order to determine the nanoparticle biocompatibility. As shown in figure 6(C), no statistically significant cytotoxicity was detected with nanoparticles at concentrations up to 0.1 mgFe mL<sup>-1</sup>, 0.02 mgBi mL<sup>-1</sup>. However, concentrations of 0.5 mgFe mL<sup>-1</sup>, 0.1 mgBi mL<sup>-1</sup> caused relatively small but statistically significant cytotoxicity ( $P$  < 0.05) related to untreated control cells. Moreover, the results obtained by the trypan blue exclusion test, used as the second assay to measure cell viability, confirmed the biocompatibility of the nanoparticles analyzed. The cell survival rate was up to 97% for all the samples. The values obtained that represent the mean of three different experiments  $\pm$ SD were  $99.3 \pm 3.7$  for the control cells and  $98.7 \pm 5.1$ ,  $97.9 \pm 5.2$  and  $97.7 \pm 5.1$  for the nanoparticle concentrations in increasing order. The statistical analysis showed no significant toxicity ( $P$  > 0.05). In summary, our results showed appropriate biological properties for FeBi@SiPEG nanoparticles in cell cultures, which makes them promising candidates for their use *in vivo*: (i) they are biocompatible and (ii) they do not accumulate in large amounts into cells.

### 3.4. Dual image study

In figure 7 the  $\mu$ CT and MRI images acquired after a subcutaneous injection of FeBi@SiPEG into the left leg of a mouse are compared. The MRI images present a diffuse contour of the zone where the contrast was injected and make the observation of the surrounding areas impossible. In contrast to that, the  $\mu$ CT enables a precise determination of the location of the contrast and its concentration (red arrow in the coronal  $\mu$ CT image) or its absence if an air bubble is accidentally injected (red arrow in the axial  $\mu$ CT image). It is clear that the combination of  $\mu$ CT in the presence of bismuth enables a clear outline of the location of the contrast, whereas the MRI images were useless due to the artifacts caused by the high local concentration.

## 4. Discussion

Cell cultures have become the first indispensable step to evaluate nanoparticle effectiveness and safety and are used for pre-screening nanomaterials before *in vivo* analysis.



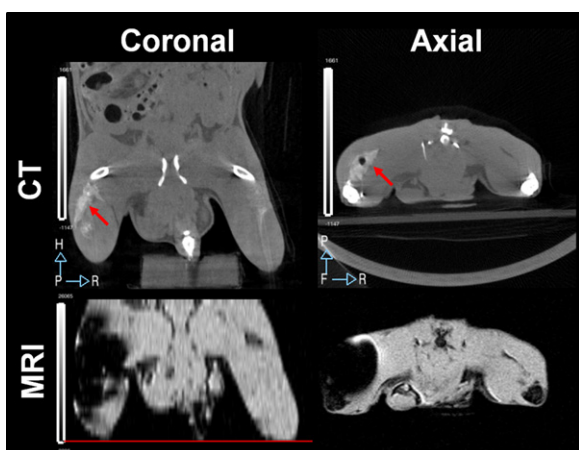


**Figure 7.** Coronal and axial images taken by CT and MRI after the subcutaneous administration of 100  $\mu\text{L}$  of FeBi@SiPEG (157 mM Fe and 14.6 mM Bi). The location of the contrast in the left leg of the mouse was marked with an arrow in the CT pictures. The black dot is an air bubble accidentally injected.

Regarding this fact, successive revisions have proposed the need for assess *in vitro* toxicity of nanoparticles [26–29]. The results presented here indicate that FeBi@SiPEG did not induce high toxicity in HeLa cells assayed by the MTT test (surviving fraction >90%). However, cells exposed 24 h to FeBi@SiPEG at the highest concentration used (0.5 mgFe mL<sup>-1</sup>, 0.1 mgBi mL<sup>-1</sup>) showed minimal but statistically significant dose-dependent toxicity. These results were similar to those obtained for pure magnetite first coated with dimercaptosuccinic acid and then modified with PEG polymers at the same iron concentration [30] and could not be attributed to the liberation of ionic bismuth. Taking into account that morphological changes that could indicate an apoptotic cell response were not detected, the low toxicity at this concentration detected by a MTT metabolic activity assay could be attributed to a temporary alteration of cellular metabolism that was probably due to FeBi@SiPEG nanocrystals that adhered to the cell's surface which could affect the MTT result and not to the induction of irreversible cellular damage. Trypan blue exclusion has been proposed as the gold standard method to validate cell viability after magnetic nanoparticle incubation [31]. The results obtained using a trypan blue assay for cell count in a ferrozine assay confirmed the biocompatibility of FeBi@SiPEG nanocrystals, and the cell survival was >96% after 24 h incubation with 0.5 mgFe mL<sup>-1</sup>, 0.1 mgBi mL<sup>-1</sup>.

The low cytotoxicity of iron oxide nanoparticles has been reported on extensively; see, for example, [32, 33]. Moreover, previous studies have reported that iron oxide nanoparticles PEG coating reduce ROS formation and therefore, may prevent cell toxicity [34]. In contrast, there are few studies on the biocompatibility of bismuth nanoparticles. Luo *et al* [35] described that bismuth nanoparticles are non-toxic on HeLa cells after 24 h of incubation with 10<sup>-7</sup> mgBi mL<sup>-1</sup>, but at higher concentrations (10<sup>-5</sup> mgBi mL<sup>-1</sup>) modified bismuth nanoparticles with either silica, amine modified silica or polyethylene glycol were able to kill HeLa cells, and the

degree of cytotoxicity depended on the specific surface modification [35]. More recently, Song *et al* [36] described the biological effects of bismuth ferrite nanoparticles (size range of 30–90 nm) in PC12 cells. These authors reported (MTT) that cytotoxicity was dose-dependent, with increasing exposure concentrations from 0.01 to 0.2 mg Bi/mL and reached 65% when the nanoparticle concentration was 0.5 mg Bi/mL [36].

Toxicity is a big issue concerning the systemic administration of bismuth compounds [37, 38] even though this element is considered 'green' in comparison with other heavy metals [39]. The  $LD_{66}$  of several ionic bismuth compounds injected intravenously was determined in rabbits as 4.5 mgBi Kg<sup>-1</sup> B.W. (sobismol®), 2.5 mgBi Kg<sup>-1</sup> B.W. (bismuth citrate) and 3.5 mgBi Kg<sup>-1</sup> B.W. (bismuth thioglycollate) [40]. For a comparison the  $LD_{50}$  of uncoated iron oxide nanoparticles of 9 nm size intravenously injected was reported recently as 163.6 mgFe Kg<sup>-1</sup> B.W. in mice [41]. For intramuscular administration it has been reported that the toxicity of ionic bismuth was reduced with respect to the intravenous injection, and, for example, 85 mgBi Kg<sup>-1</sup> B.W. (bismuth citrate) in rabbits is considered non-toxic [42].

In general terms the toxicity of bismuth compounds administered by intramuscular injection is highly dependent on their solubility in water [37]. Previous works reported that the use of bismuth sulphide nanomaterials as CT contrast agents is justified by the extremely low solubility of Bi<sub>2</sub>S<sub>3</sub> ( $K_{ps} = 1.82 \cdot 10^{-99}$  [43]) that enables the use of doses as high as 340 mgBi Kg<sup>-1</sup> B.W. of intravenous injection [10]. The solubility of bismuth oxide at a neutral pH is 4.5 · 10<sup>-6</sup> M, corresponding to a solubility product of 5 · 10<sup>-38</sup> [44], which is much higher than that for bismuth sulphide but is low enough to justify the low cytotoxicity of the nanocrystals prepared in this work. Although we could not detect appreciable dissolution of FeBi nanocrystals in water under sonication *in vitro* [15], and we used a silica coating to further reduce the bismuth leakage, we limited in this work the doses of bismuth to 10 mgBi Kg<sup>-1</sup> B.W., which has been considered safe for daily oral administration (bismuth subgallate) [37] or tolerated for intramuscular injection (bismuth citrate) [40].

Similar materials to what was proposed in this work are the dual CT/MRI contrasts core-shell Fe<sub>2</sub>O<sub>3</sub>@Au [45] and Fe<sub>2</sub>O<sub>3</sub>@TaO<sub>x</sub> [5], but both show transversal relaxivity values of 95 and 82 mMFe<sup>-1</sup> s<sup>-1</sup>, respectively, which are smaller than the one reported in this work (175 mMFe<sup>-1</sup> s<sup>-1</sup>). This is probably related to the need for a larger proportion of an x-ray absorptive element to achieve CT contrast with elements with lower x-ray absorptivities than bismuth. In a recent paper dextran-coated bismuth-iron oxide was tested as double contrasts for CT and MRI; they obtained good CT contrast due to the higher bismuth proportion (16%) but with low transversal relaxivity (0.4 mMFe<sup>-1</sup> s<sup>-1</sup>) [46].

Instead of the concept of dual contrast agent able to give contrast by CT and MRI (references [5] and [45] are better options for this), we propose the incorporation of a limited amount of bismuth on a superparamagnetic MRI contrast (bismuth labeling), that without reduction in relaxivity and increase in toxicity could enable the CT assessment of the

local delivery of magnetic nanoparticles via intramuscular or intratumoral injection [47]. In general, systemically administered magnetic nanoparticles, even those functionalized with antibodies that specifically bind to the targeted tumor, do not result in enough of an accumulation to ensure a therapeutic dose at the tumor site, and local administration is preferable. In the case of hyperthermia treatments, the clinical strategy usually consists of the implantation or intratumoral injection of a concentrated suspension of magnetite nanoparticles [48]. The first study on the feasibility of thermotherapy using magnetic nanoparticles in human patients was conducted by Andreas Jordan at Berlin's Charité Hospital, which was administered via intratumoral 0.1–0.7 mL of aqueous dispersion of 15 nm iron oxide nanoparticles at a concentration as high as 112 mgFe mL<sup>-1</sup> [49]. At such an iron concentration, the NMR image is distorted, and the CT will be more convenient for the assessment of the distribution of the nanoparticles into the tumor. The use of FeBi nanocrystals that combine a high magnetic response and the possibility of accurate detection of the bismuth shell by CT in the early stages and by MRI in the latest, showing the final fate of the nanoparticles, could represent a good improvement in the treatment of cancer using magnetic carriers.

## 5. Conclusions

A bismuth-labeled magnetic colloid able to be detected by CT and MRI was made using PEG-coated core-shell iron oxide-bismuth oxide nanocomposite hybrid nanoparticles. Although the bismuth content retained at the nanoparticle's surface after the coating is around 8% on a molar basis, the higher x-ray opacity of bismuth makes the contrast CT images possible, and due to the superparamagnetic nature of the core, these nanoparticles also behave as a SPIO contrast agent for MRI. In spite of the high spatial resolution of both medical image techniques, the presence of artifacts in the MRI due to high local iron concentrations makes the CT and MRI images nonequivalent, making the CT image more suitable at high concentrations and the MRI suitable at low ones. Bismuth-labeled magnetic nanomaterials, as proposed in this work, when included in a theranostic nanoplatform, could be detected in the tumor at the initial stages of the drug delivery process by CT and in the distal organs by MRI afterward, greatly improving the traceability of the nanoparticles in the organism, which is an important limitation in the translation of nanoparticles into clinical practice.

## Acknowledgments

This work was supported by the Spanish Ministry of Economy and Competitiveness through Project MAT2011-23641. The authors acknowledge the help of Dr Ruiz Cabello and Dr Herranz in the relaxometric measurements at the Centro Nacional de Investigaciones Cardiovasculares CNIC and acknowledge Guerbet Group for the economic support and the supply of Xenetix®. The research at ORNL US, the

Department of Energy (DOE), Basic Energy Sciences (BES), the Materials Sciences and Energy Division (MV) and the Complutense University of Madrid (UCM) was supported by the ERC Starting Investigator Award STEMOX 739239.

## References

- [1] Longmire M, Choyke P L and Kobayashi H 2008 Clearance properties of nano-sized particles and molecules as imaging agents: consideration and caveats *Nanomedicine* **3** 703–17
- [2] Liu Y, Ai K and Lu L 2012 Nanoparticulate x-ray computed tomography contrast agents: from design validation to *in vivo* applications *Acc. Chem. Res.* **45** 1817–27
- [3] De Vries A, Custers E, Lub J, van der Bosch S, Nicolay K and Grill H 2010 Block-copolymer stabilized iodinated emulsions for use as CT contrast agents *Biomaterials* **31** 6537–44
- [4] Hainfeld J F, Slatkin D N, Focella T M and Smilowitz H M 2006 Gold nanoparticles: a new x-ray contrast agent *Br. J. Radiol.* **79** 248–53
- [5] Lee N *et al* 2012 Multifunctional Fe<sub>3</sub>O<sub>4</sub>/TaO<sub>x</sub> core/shell nanoparticles for simultaneous magnetic resonance imaging and x-ray computed tomography *J. Am. Chem. Soc.* **134** 10309–12
- [6] Chou S W, Shau Y H, Wu P C, Yang Y S, Shieh D B and Chen C C. 2010 *In vitro* and *in vivo* studies of FePt nanoparticles for dual modal CT/MRI molecular imaging *J. Am. Chem. Soc.* **132** 13270–8
- [7] Pan D *et al* 2009 Detecting vascular biosignatures with a colloidal radio-opaque polymeric nanoparticle *J. Am. Chem. Soc.* **131** 15522–7
- [8] Rabin O, Perez J M, Grimm J, Wojtkiewicz G and Weissleder R 2006 An x-ray computed tomography imaging agent based on long-circulating bismuth sulphide nanoparticles *Nat. Mat.* **5** 118–22
- [9] Ai K L, Liu Y L, Liu J H, Yuan Q H, He Y Y and Lu L H 2011 Large-scale synthesis of Bi<sub>2</sub>S<sub>3</sub> nanodots as a contrast agent for *in vivo* x-ray computed tomography imaging *Adv. Mater.* **23** 4886–91
- [10] Kinsella J M *et al* 2011 X-ray Computed tomography imaging of breast cancer by using targeted peptide-labeled bismuth sulphide nanoparticles *Angew. Chem. Int. Ed.* **50** 12308–11
- [11] Fang Y *et al* 2013 Dendrimer-stabilized bismuth sulfide nanoparticles: synthesis, characterization, and potential computed tomography imaging applications *Analyst* **138** 3172–80
- [12] Li J *et al* 2013 Topological insulator bismuth selenide as a theranostic platform for simultaneous cancer imaging and therapy *Sci. Rep.* **3** 1998
- [13] Rivera E J *et al* 2013 Bismuth@US-tubes as a potential contrast agent for x-ray imaging applications *J. Mater. Chem. B* **1** 4792–800
- [14] Mattei J G *et al* 2013 Formation of bimetallic FeBi nanostructured particles: investigation of a complex growth mechanism *J. Phys. Chem. C* **117** 1477–84
- [15] Andres-Verges M, Morales M P, Veintemillas-Verdaguer S, Palomares F J and Serna C J 2012 Core/shell magnetite/bismuth oxide nanocrystals with tunable size, colloidal and magnetic properties *Chem. Mater.* **24** 319–24
- [16] Abella M *et al* 2012 Software architecture for multi-bed FDK-based reconstruction in x-ray CT scanners *Comput. Methods Programs Biomed.* **107** 218–32
- [17] Riemer J, Hoepken H H, Czerwinska H, Robinson S R and Dringen R 2004 Colorimetric ferrozine-based assay for the quantitation of iron in cultured cells *Anal. Biochem.* **331** 370–5

- [18] Mosmann T 1983 Rapid colorimetric assay for cellular growth and survival: application to proliferation and cytotoxicity assays *J. Immunol. Methods* **65** 55–63
- [19] Laguna-Marco M A *et al* 2014 Structural determination of Bi-doped magnetite multifunctional nanoparticles for contrast imaging *Phys. Chem. Chem. Phys.* **16** 18301–10
- [20] Rodriguez-Carvajal J 2001 Recent developments of the program FULLPROF, in commission on powder diffraction (IUCr) *Newsletter* **26** 12–9 (<http://journals.iucr.org/iucr-top/comm/cpd/Newsletters/>)
- [21] Prekajski M *et al* 2010 Room-temperature synthesis of nanometric  $\alpha$ - $\text{Bi}_2\text{O}_3$  *Mat. Lett.* **64** 2247–50
- [22] Jørgensen J E, Mosegaard L, Thomsen L E, Jensen T R and Hanson J C 2007 Formation of  $\gamma$ - $\text{Fe}_2\text{O}_3$  nanoparticles and vacancy ordering: an *in situ* x-ray powder diffraction study *J. Sol. State. Chem.* **180** 180–5
- [23] Miyazawa T, Fukushima K and Ideguchi Y 1962 Molecular vibrations and structure of high polymers. III. Polarized infrared spectra, normal vibrations, and helical conformation of polyethylene glycol *J. Chem. Phys.* **37** 2764–76
- [24] Cullity B D and Graham C D 2011 *Introduction to Magnetic Materials* 2nd edn (New Jersey: Wiley)
- [25] Corot C, Robert P, Idée J M and Port M 2006 Recent advances in iron oxide nanocrystal technology for medical imaging *Adv. Drug Deliver. Rev.* **58** 1471–504
- [26] Lewinski N, Colvin V and Drezek R 2008 Cytotoxicity of nanoparticles *Small* **4** 26–49
- [27] Arora S, Rajwade J M and Paknikar K M 2012 Nanotoxicology and *in vitro* studies: the need of the hour *Toxicol. Appl. Pharmacol.* **258** 151–65
- [28] Elsaesser A and Howard C V 2012 Toxicology of nanoparticles *Adv. Drug Deliv. Rev.* **64** 129–37
- [29] Sarkar A, Ghosh M and Sil P C 2014 Nanotoxicity: oxidative stress mediated toxicity of metal and metal oxide nanoparticles *J. Nanosci. Nanotechnol.* **14** 730–43
- [30] Ruiz A *et al* 2013 Short-chain PEG molecules strongly bound to magnetic nanoparticle for MRI long circulating agents *Acta Biomater.* **9** 6421–30
- [31] Hoskins C, Wang L, Cheng W P and Cuschieri A 2012 Dilemmas in the reliable estimation of the in-vitro cell viability in magnetic nanoparticle engineering: which tests and what protocols *Nanoscale Res. Lett.* **7** 77
- [32] Villanueva A *et al* 2009 The influence of surface functionalization on the enhanced internalization of magnetic nanoparticles in cancer cells *Nanotechnology* **20** 115103
- [33] Calero M *et al* 2014 A efficient and safe internalization of magnetic iron oxide nanoparticles: two fundamental requirements for biomedical applications *Nanomed. Nanotechnol. Biol. Med.* **10** 733–43
- [34] Yu M, Huang S, Yu K J and Clyne A M 2012 Dextran and polymer polyethylene glycol (PEG) coating reduce both 5 and 30 nm iron oxide nanoparticle cytotoxicity in 2D and 3D cell culture *Int. J. Mol. Sci.* **13** 5554–70
- [35] Luo Y, Wang C, Qiao Y, Hossain M, Ma L and Su M 2012 *In vitro* cytotoxicity of surface modified bismuth nanoparticles *J. Mater. Sci. Mater. Med.* **23** 2563–73
- [36] Song Q *et al* 2014 The acute cytotoxicity of bismuth ferrite nanoparticles on PC12 cells *J. Nanopart. Res.* **16** 2408
- [37] Bradley B, Singleton M and Wan P A L 1989 Bismuth toxicity- a reassessment *J. Clin. Pharm. Ther.* **14** 423–41
- [38] Slikkerveer A and Wolff F A 1989 Pharmacokinetics and toxicity of bismuth compounds *Med. Toxicol. Adverse Drug Exp.* **4** 303–23
- [39] Moham R 2010 Green Bismuth *Nat. Chem.* **2** 336
- [40] Sollmann T and Seifter J 1942 Intravenous injections of soluble bismuth compounds: their toxicity, and their sojourn in the blood and organs *J. Pharmacol. Exp. Ther.* **74** 134–54
- [41] Zhao S H *et al* 2012 The *in vivo* investigation of  $\text{Fe}_3\text{O}_4$  nanoparticles acute toxicity in mice *Biomed. Eng-Appl. Basis. Commun.* **24** 229–35
- [42] Leonard C S 1926 Studies in the pharmacology of bismuth salts II. Toxicity and urinary elimination of soluble bismuth salts *J. Pharmacol. Exp. Ther.* **28** 89–108
- [43] Linde D R (ed) 1991 *CRC Handbook of Chemistry and Physics* 72nd edn (Florida: CRC Press)
- [44] Bidleman F T 1971 Bismut-ditizone equilibria and hydrolysis of bismuth ion in aqueous solution *Anal. Chim. Acta* **56** 221–31
- [45] Zhang S, Qi Y Y, Yang H, Gong M F, Zhang D and Zou L G 2013 Optimization of the composition of bimetallic core/shell  $\text{Fe}_2\text{O}_3/\text{Au}$  nanoparticles for MRI/CT dual-mode imaging *J. Nanopart. Res.* **15** 2023
- [46] Naha P C *et al* 2014 Dextran coated bismuth-iron oxide nanohybrid contrast agents for computed tomography and magnetic resonance imaging *J. Mater. Chem. B* **2** 8239–48
- [47] Tu S J, Wu S Y, Wang F S and Ma Y H 2014 Retention assessment of magnetic nanoparticles in rat arteries with micro-computed tomography *Phys. Med. Biol.* **59** 1271–81
- [48] Ortega D and Pankhurst Q A 2013 *Magnetic Hyperthermia Nanoscience: Volume 1: Nanostructures through Chemistry* ed P O'Brien (Cambridge: Royal Society of Chemistry) pp 60–88
- [49] Maier-Hauff K *et al* 2007 Intracranial thermography using magnetic nanoparticles combined with external beam radiotherapy: results of a feasibility study on patients with glioblastoma multiforme *J. Neuro-Oncol.* **81** 53–60